Investigating Different Priors for Image Deconvolution in Histopathology Images

Vishwesh Ramanathan

Abstract—Histopathology images are digital scans of tissue slides scanned at multiple and very high magnifications. However, the digital scanners used to scan these slides are very susceptible to irregularities such as small bumps, specks of dust, or foreign particles, leading to out-of-focus. Deconvolution may potentially correct the out-of-focus regions. In this work, we study the effects of different priors in the context of non-blind deconvolution using Adam Optimizer. We also propose three new regularizers, perform extensive quantitative and qualitative analyses and discuss the observations.

Index Terms—Computational Imaging, Histopathology, Non-Blind Deconvolution

1 Introduction

The digitization of histopathology slides has ushered in the rise of computer aided analyses and interpretation of histopathology images. These algorithms potentially help pathologists in many of their day-to-day work by performing tasks such as cell detection [1], [2], registration [3], survival analysis [4], [5] etc. However, these algorithms require high-quality digital images. The digital images from a tissue slide are often formed by powerful digital scanners which are able to capture microscopic entities with a high resolution of $0.2\frac{\mu m}{pixel}$. The images are captured in a pyradimical format as shown in figure 1, at different resolutions, to aid pathologists who often look at the tissue slides at multiple resolutions for diagnosis. Due to such high magnification power, these scanners are very susceptible. Irregularities in the tissue resection such as small bumps, small specs of dust, or foreign object, can cause scanners to go out of focus leading to blurred scan, which has to again be rescanned. This can be very costly due to the time it takes to prepare slides and scan.

Image deconvolution is an actively studied field in computer vision. The field assumes the following image formation model

$$\vec{b} = \vec{a} * \vec{x} + \eta \tag{1}$$

Where $\vec{b}$ is the procured image that is blurred. The true in-focus image $\vec{x}$ undergoes convolution using some blur kernel $\vec{a}$ and is corrupted with some noise η. There are two types of deconvolution problems, blind and non-blind. Typically, in a non-blind image deconvolution problem, the blur kernel is known apriori, hence one can potentially solve the inverse problem using the image formation model. However, the solution is not trivial, as it is an ill-posed problem with many existing solutions. To converge to a solution, lot of different types of priors has been proposed for natural images, however it is not immediately clear if the same assumptions upholds for other kinds of images such as histopathology images. For this study, we are interested in knowing the effects of popular priors or regularizers in the deconvolution of histopathology images. We restrict ourselves to only non-blind deconvolution with a known blur kernel. We solve equation 1 using Adam optimization [6], and in the end, propose three novel priors and explore their effects.

Email: vishwesh.ramanathan@mail.utoronto.ca
Code is available at https://github.com/Vishwesh4/PriorsDeconvolution

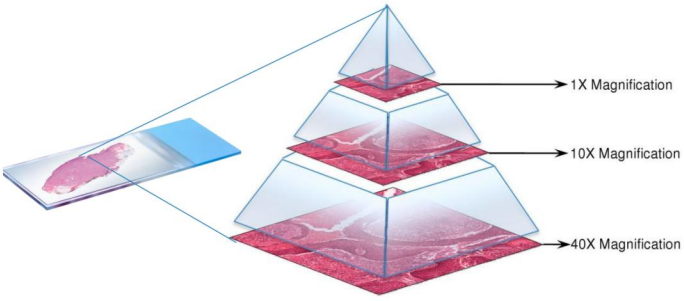

Fig. 1: Pyramid structure of a digital scan from a tissue slide

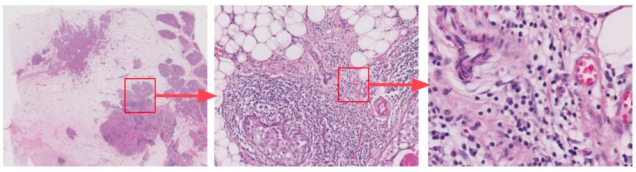

Fig. 2: Different resolutions in histopathology images

2 Related Work

There have been a lot of different types of priors or regularizers proposed for the inverse problem. Total Variation [7], a popular regularizer, works based on the assumption that gradients of images are sparse. Although it works well for natural images, it produces staircase effect [8], especially for medical images. There have also been works that have used laplacian norm [9] and L1 norm [9], which has been shown to work well in astronomy. Recently, Hessian Schatten Norm [10] was used as a prior in [11], which was shown to work very well in deconvolution in fluorescence imaging. For digital pathology, blind deconvolution using deep learning [12] was performed, however no regularizers were used

Regularizers	$\Psi(\mathbf{x})$
Anisotropic Total Variation	$\sum_{j\in\Omega} \|\|\mathcal{D}_j\mathbf{x}_j\|\|_1$
Isotropic Total Variation	$\sum_{j\in\Omega} \|\|\mathcal{D}_j\mathbf{x}_j\|\|_2$
L1	$\sum_{j\in\Omega} \|\|\mathbf{x}_j\|\|_1$
L2	$\sqrt{\sum_{j\in\Omega} \mathbf{x}_j^2}$
Laplacian	$\sum_{j\in\Omega}((\mathcal{H}_{xx}\mathbf{x})_j + (\mathcal{H}_{yy}\mathbf{x})_j)^2$
Hessian Schatten norm	$\sum_{j\in\Omega} \|\|\mathcal{H}_j\mathbf{x}\|\|_F$
Maximize cells (proposed)	$-(\textit{Number of cells})$
Cross Entropy (proposed)	$-log(T(\mathbf{x}\in\mathbb{P}\|\mathbf{x}))$
KL Divergence (proposed)	$-(T(\mathbf{x}\in\mathbb{P}\|\mathbf{x}) - T(\mathbf{b}\in\mathbb{Q}\|\mathbf{b}))$

TABLE 1: Table of different regularizers used in the report. Here $\mathcal{D}$ denotes first-order differentiation and $\mathcal{H}$, the Hessian of the image. $\mathbb{P}$ and $\mathbb{Q}$ refer to the in-focus and out of focus distribution. Ω is the set of all pixels in an image. F is the Frobenius norm, and T is a neural network that does binary classification between in-focus and out-of-focus distribution

in the work. To the best of my knowledge, there is no documentation of the performance of different priors in histopathology images.

3 Proposed Method

In this work, we implement 6 popular priors and 3 novel priors, as shown in table 1. We blurred in-focus images with different kernels and noise for the experiments using image formation equation 1. We solved non-blind deconvolution using the following loss function

$$\min_x \frac{1}{2}||\mathbf{A}\mathbf{x} - \mathbf{b}||^2{}_2 + \lambda\Psi(\mathbf{x}) \tag{2}$$

We solve the loss function 2 using Adam optimizer and use different priors mentioned in 1, with different importance factor λ. In the next section, we discuss the three proposed priors

3.1 Maximize Cells

Histopathology images usually have a lot of cells. We often need a high level of separation between each cell. Hence, we hypothesize maximizing the number of cells would enforce the deconvolution to dissect individual cells from their surrounding cells, which otherwise would have been a single clump due to the blur. This should also encourage sharp edges for each individual cell.

These cells, although having a variety of shapes, can be roughly approximated as round entities. It is further assumed that their diameter is $8\mu m$ [13]. We wish to calculate the number of cells approximately given $\mathbf{x}$ and maximize it over the iterations. We estimate the number of cells over three steps as shown in figure 3. Given $\mathbf{x}$, we first construct an edge map using Canny edge detector [14]. This is done to reduce noise and focus on sharpening the edges of the cells. Once we obtain the edge map, we convolve the edge map with three handcrafted filters as shown in figure 3. The filters are designed to give high activations when the center of the filter is around the center of the cells in the edge map. Since we use histopathology images at a resolution of $0.5\frac{\mu m}{pixel}$, we use filters with circular and elliptical shapes with a diameter of $8\mu m$. Along with positive values outlining the boundaries, we put negative values around the center to give low or 0 activations when not around the center. We perform convolutions using circular and two elliptical filters to account for different orientations and shapes. Finally, we normalize the activations and threshold values at around 70% quantile. We sum up the resultant output and take an average over the three filters to estimate the number of cells. Finally in equation 2, we use the following regularizer

$$\Psi(\mathbf{x}) = -(\textit{Number of cells}) \tag{3}$$

3.2 Cross Entropy

Let there be two distributions $\mathbb{P}$ and $\mathbb{Q}$, such that all in-focus images or $\mathbf{x}$ belongs to in-focus distribution $\mathbb{P}$, and all blurry/out-of-focus images or $\mathbf{b}$ belong to out-of-focus distribution $\mathbb{Q}$. Using the two sets of images, we trained a Resnet18 [15] for binary classification to predict in-focus versus out-of-focus. The model outputs the class probabilities given an image in the inference stage. Hence, we can use the class probabilities from the trained network to evaluate the quality of the deconvolved image $\mathbf{x}$ each iteration. Defining the regularizer as

$$\Psi(\mathbf{x}) = -log(T(\mathbf{x}\in\mathbb{P}|\mathbf{x})) \tag{4}$$

Where T is our trained network. $\Psi(\mathbf{x})$ will be 0 for perfectly restored image $\hat{\mathbf{x}}$ and ∞ for badly restored image. Hence the regularizer should ideally push $\mathbf{x}$ as close to the in-focus distribution $\mathbb{P}$ as possible.

3.3 KL Divergence

We also use KL divergence as a regularizer and wish to maximize the KL divergence between the restored images $\mathbf{x}$, which should ideally belong to in-focus distribution $\mathbb{P}$ and the blurred images $\mathbf{b}$ which belong to out-focus distribution $\mathbb{Q}$. Defining the regularizer as

$$\Psi(\mathbf{x}) = -D_{KL}(\mathbf{x}||\mathbf{b}) \tag{5}$$

To calculate KL divergence, we use the Donsker Varadhan Representation [16]. We have

$$D_{KL}(\mathbb{P}||\mathbb{Q}) = sup_{T:\Omega\to\mathbb{R}}\mathbb{E}_{\mathbb{P}}[T] - log(E_{\mathbb{Q}}[e^T]) \tag{6}$$

Where T is a neural network, which takes input samples from $\mathbb{P}$ in the left term and input samples from $\mathbb{Q}$ in the right term. In our case, we have only a single sample. We can also reuse the trained network from the cross-entropy regularizer. Using this, we can simplify the expression to this

$$D_{KL}(\mathbb{P}||\mathbb{Q}) \geq T(\mathbf{x}\in\mathbb{P}|\mathbf{x}) - T(\mathbf{b}\in\mathbb{Q}|\mathbf{b})) \tag{7}$$

$$\Psi(\mathbf{x}) = -(T(\mathbf{x}\in\mathbb{P}|\mathbf{x}) - T(\mathbf{b}\in\mathbb{Q}|\mathbf{b})) \tag{8}$$

Notice we have $\geq$ because we did not optimize T on the loss equation 6. However, we can still use this estimate as a regularizer. The KL divergence should be -1 if $\mathbf{x}$ is not restored correctly and 1 if $\mathbf{x}$ is adequately restored.

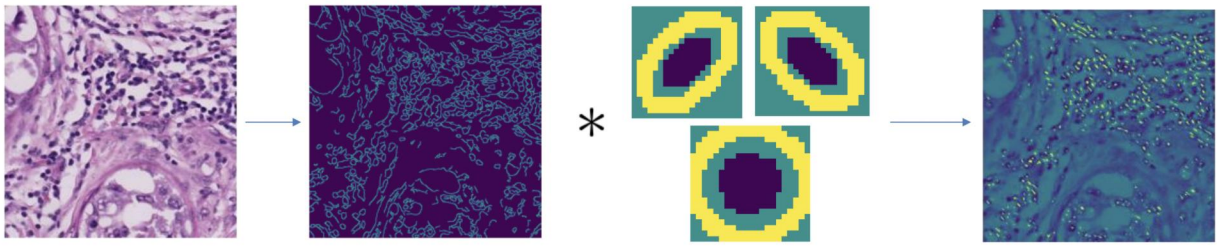

Fig. 3: Maximize cell regularize. We generate an edge map and convolved it with three handcrafted filters. For the filters, yellow indicates 1, green indicates 0, and purple indicates -1. The right-most figure indicates the activation map overlayed on top of the original image

4 Experimental Results

4.1 Experimental Details

For the experiments, over 24000 patches of size 256×256 were extracted from a single histopathology image at a resolution of $0.5\frac{\mu m}{pixel}$. The histology image is taken from the publically available TIGER dataset [17]. The patches were extracted at a regular stride to sample all the different types of tissues and explore the effects of deconvolution. The patches were divided into training and test set. The network T was trained using the training set, and the evaluations were performed on 150 samples from the test set.

We also varied different hyperparameters for the experiments to observe their effects on the regularizers. We tried a combination of 3 blur kernels with varying filter sizes and standard deviations. We also tried 2 different sets of λ and noise η.

For Cross-entropy and KL divergence regularizers, we trained the network T on the training samples. For generating the dataset for training, the in-focus samples were corrupted synthetically using the image formation model 1. Three datasets were generated for each blur kernel to train three different networks T. The datasets were also corrupted with noise with varying standard deviations to avoid overfitting to a particular noise level. Overall the models were trained to achieve 98% accuracy in the test set.

4.2 Results

The qualitative results are shown in figure 4 and figure 5, and the quantitative results are shown in table 2, table 3, table 4 and table 5. We observe lot of interesting properties in the experiments.

Observation 1: Implicit bias of gradient descent

The implicit bias of gradient descent has been well studied [18], where it has been shown that gradient descent and stochastic gradient descent converge to minimum L_2 norm solution. The work [19] further proves that Adam optimizer has a similar implicit bias. We can also observe this phenomenon from our results in table 2 and table 3, where the results are the same for both L_2 and no prior.

Observation 2: There is no significant effect of Maximize cells, Cross Entropy, and KL divergence prior

We observe no significant effect of the proposed priors compared to using no prior as seen quantitatively. This may be happening due to the design of the regularizer. We observe that although the proposed regularizers give high values for blurry images and low values for perfectly reconstructed images, they do not significantly affect the gradient descent trajectory. That is, the trajectory of the gradient descent taken in the no prior case would simultaneously minimize the values of the proposed regularizers. Hence this, in effect, does not change the gradient trajectory. This causes the regularizers to converge to the same solution as no prior.

Observation 3: Qualitatively, No prior, Maximize cells, L1, Cross entropy, and KL divergence, does not denoise the image well, leading to low values of image metrics

We observe that No prior, Maximize cells, L1, Cross entropy, and KL divergence do not denoise the image well. Although qualitatively as shown in figure 4 and figure 5, the image may seem to be of good quality with refined edges; however, it is grainy. This graininess leads to low values in image metrics such as PSNR and SSIM, compared to regularizers such as TV priors and Hessian Schatten (due to sparse first-order gradients), which give blurry images but high PSNR and SSIM values.

Observation 4: The regularizers give different results for different areas in a histopathology image

We confirm this qualitatively using figure 4 and figure 5. Figure 4 is taken from an area with high cell density where the lymphocytes surround the tumor cells. Figure 5 is taken from an area with fat tissues. We observe qualitatively for figure 4, TV prior and Hessian Schatten perform worse than other regularizers such as Laplacian, proposed priors, and even no prior. However, figure 5 shows the opposite effect where TV priors and Hessian Schatten perform better. This may be happening because TV priors and Hessian Schatten are based on the assumption that the first-order gradients should be sparse. This may be generally true for natural images but fails for histopathology in cases such as figure 4, where the density of cells is high, leading to non-sparse first-order gradients. Since the assumptions uphold for figure 5, the regularizers perform better.

Observation 5: No prior, three proposed priors, laplacian are better than TV and Hessian Schatten at low noise levels

The observation is very similar to observation 3. No prior, three proposed priors and laplacian regularizers lead to sharp but grainy deconvolutions compared to TV and Hessian Schatten. As the noise level increases, the graininess

decreases; hence the former regularizers overtake the latter regularizers quantitatively, as shown by PSNR and SSIM image metrics.

Observation 6: Different blur kernel and λ has varied effects on different regularizers

We observe different effects of blur kernel and λ for different regularizers. For example, we see a drop in TV priors and Hessian Schatten with increasing blur kernel size and standard deviation, as compared to other regularizers such as Laplacian.

5 Conclusion

In this work, we investigate 6 popular priors and also proposed three new priors. We investigated their properties quantitatively and qualitatively and stated many interesting observations. For future work, it would be interesting to try multiple regularizers to account for individual weaknesses. From this study, we also realized the importance of taking the implicit bias of the gradient descent into account while designing new priors so as to converge to different and better local minima.

6 Acknowledgements

I would like to thank Shayan Shekarforoush for his mentoring and useful comments.

References

[1] S. Graham, Q. D. Vu, S. E. A. Raza, A. Azam, Y. W. Tsang, J. T. Kwak, and N. Rajpoot, "Hover-net: Simultaneous segmentation and classification of nuclei in multi-tissue histology images," *Medical Image Analysis*, vol. 58, p. 101563, 2019.

[2] T. Chen and C. Chefd'Hotel, "Deep learning based automatic immune cell detection for immunohistochemistry images," in *International workshop on machine learning in medical imaging*. Springer, 2014, pp. 17–24.

[3] J. Chappelow, B. N. Bloch, N. Rofsky, E. Genega, R. Lenkinski, W. DeWolf, and A. Madabhushi, "Elastic registration of multimodal prostate mri and histology via multiattribute combined mutual information," *Medical physics*, vol. 38, no. 4, pp. 2005–2018, 2011.

[4] E. Wulczyn, D. F. Steiner, Z. Xu, A. Sadhwani, H. Wang, I. Flament-Auvigne, C. H. Mermel, P.-H. C. Chen, Y. Liu, and M. C. Stumpe, "Deep learning-based survival prediction for multiple cancer types using histopathology images," *PloS one*, vol. 15, no. 6, p. e0233678, 2020.

[5] R. Li, J. Yao, X. Zhu, Y. Li, and J. Huang, "Graph cnn for survival analysis on whole slide pathological images," in *International Conference on Medical Image Computing and Computer-Assisted Intervention*. Springer, 2018, pp. 174–182.

[6] D. P. Kingma and J. Ba, "Adam: A method for stochastic optimization," *arXiv preprint arXiv:1412.6980*, 2014.

[7] S. Osher, M. Burger, D. Goldfarb, J. Xu, and W. Yin, "An iterative regularization method for total variation-based image restoration," *Multiscale Modeling & Simulation*, vol. 4, no. 2, pp. 460–489, 2005.

[8] M. Lysaker, A. Lundervold, and X.-C. Tai, "Noise removal using fourth-order partial differential equation with applications to medical magnetic resonance images in space and time," *IEEE Transactions on image processing*, vol. 12, no. 12, pp. 1579–1590, 2003.

[9] "lecture7.pdf," https://www.cs.toronto.edu/~lindell/teaching/2529/slides/lecture7.pdf, (Accessed on 11/16/2022).

[10] S. Lefkimmiatis, J. P. Ward, and M. Unser, "Hessian schatten-norm regularization for linear inverse problems," *IEEE transactions on image processing*, vol. 22, no. 5, pp. 1873–1888, 2013.

[11] H. Ikoma, M. Broxton, T. Kudo, and G. Wetzstein, "A convex 3d deconvolution algorithm for low photon count fluorescence imaging," *Scientific reports*, vol. 8, no. 1, pp. 1–12, 2018.

[12] C. Jiang, J. Liao, P. Dong, Z. Ma, D. Cai, G. Zheng, Y. Liu, H. Bu, and J. Yao, "Blind deblurring for microscopic pathology images using deep learning networks," *arXiv preprint arXiv:2011.11879*, 2020.

[13] S. L. Goff, F. O. Smith, J. A. Klapper, R. Sherry, J. R. Wunderlich, S. M. Steinberg, D. White, S. A. Rosenberg, M. E. Dudley, and J. C. Yang, "Tumor infiltrating lymphocyte therapy for metastatic melanoma: analysis of tumors resected for til," *Journal of immunotherapy (Hagerstown, Md.: 1997)*, vol. 33, no. 8, p. 840, 2010.

[14] J. Canny, "A computational approach to edge detection," *IEEE Transactions on pattern analysis and machine intelligence*, no. 6, pp. 679–698, 1986.

[15] K. He, X. Zhang, S. Ren, and J. Sun, "Deep residual learning for image recognition," in *Proceedings of the IEEE conference on computer vision and pattern recognition*, 2016, pp. 770–778.

[16] M. D. Donsker and S. S. Varadhan, "Asymptotic evaluation of certain markov process expectations for large time, i," *Communications on Pure and Applied Mathematics*, vol. 28, no. 1, pp. 1–47, 1975.

[17] "Data - grand challenge," https://tiger.grand-challenge.org/Data/, (Accessed on 12/08/2022).

[18] J. Wu, D. Zou, V. Braverman, and Q. Gu, "Direction matters: On the implicit bias of stochastic gradient descent with moderate learning rate," *arXiv preprint arXiv:2011.02538*, 2020.

[19] B. Wang, Q. Meng, H. Zhang, R. Sun, W. Chen, Z.-M. Ma, and T.-Y. Liu, "Does momentum change the implicit regularization on separable data?" in *Advances in Neural Information Processing Systems*.

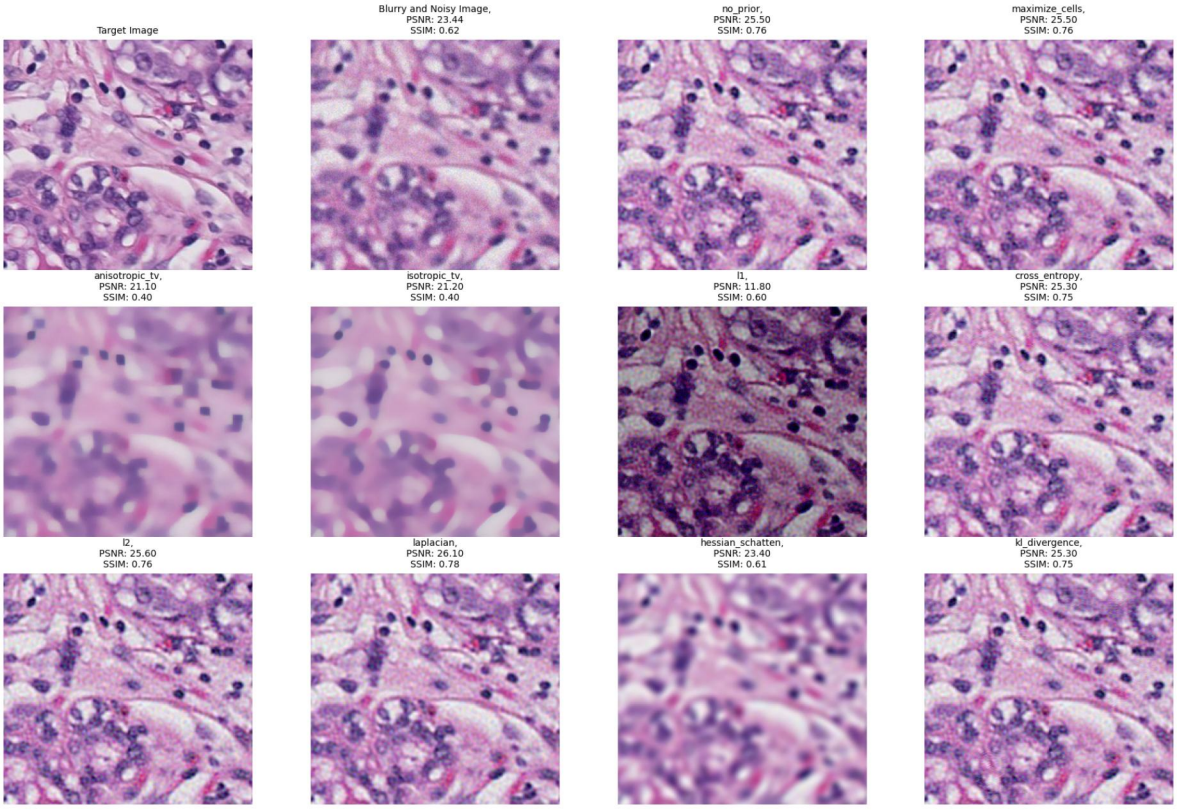

Fig. 4: Results for different regularizers on an image with high cell density. The image is blurred with a blur kernel of filter size $(10, 10)$ and standard deviation $\sigma = 1.5$. The noise standard deviation is 0.05

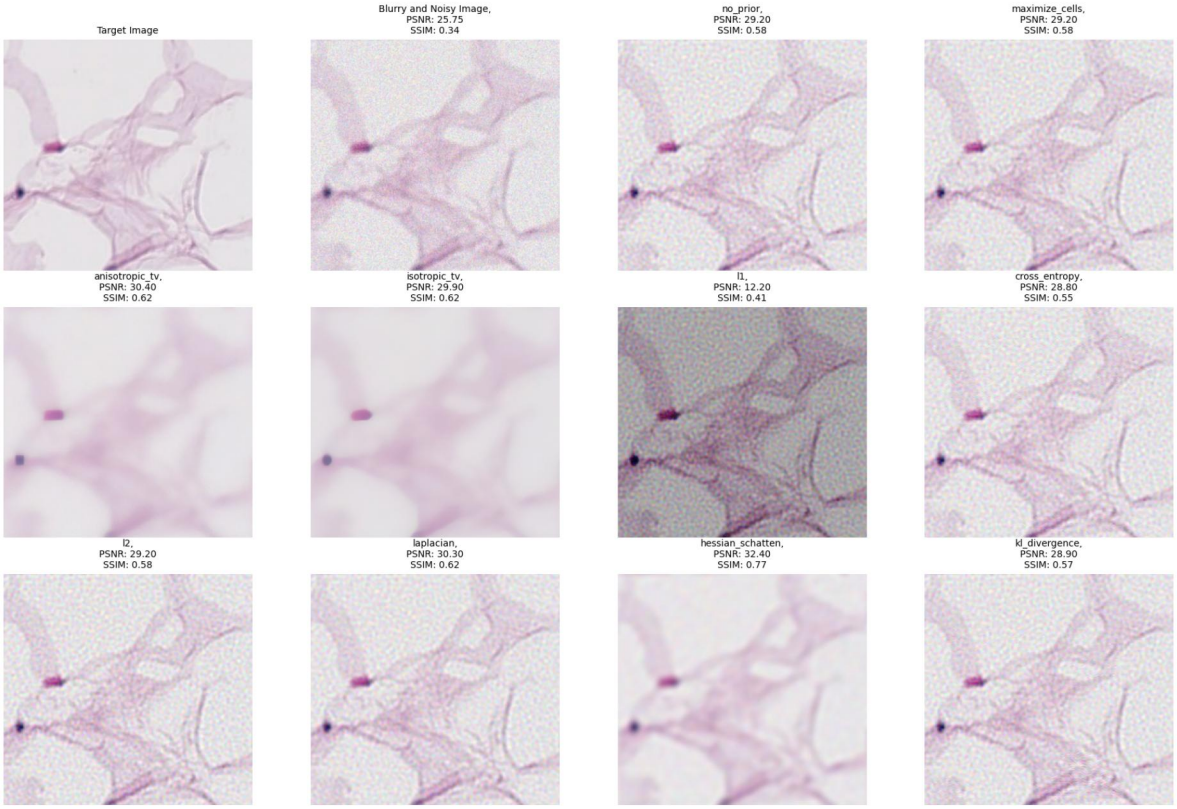

Fig. 5: Results for different regularizers on an image with fat tissue. The image is blurred with a blur kernel of filter size $(10, 10)$ and standard deviation $\sigma = 1.5$. The noise standard deviation is 0.05

Noise	Lamda	Blur Kernel	No Prior	Anisotropic TV	Isotropic TV	Hessian Schatten	L1
0.15	0.05	$(10, 10, \sigma = 1.5)$	19.49 ± 1.08	$\mathbf{26.60 \pm 2.00}$	26.16 ± 1.75	26.34 ± 1.66	19.01 ± 0.94
		$(30, 30, \sigma = 4.5)$	24.55 ± 2.47	25.45 ± 3.38	$\mathbf{25.51 \pm 3.33}$	24.87 ± 2.68	24.04 ± 2.20
		$(60, 60, \sigma = 6.5)$	24.16 ± 3.16	24.24 ± 3.54	$\mathbf{24.29 \pm 3.52}$	24.18 ± 3.22	23.71 ± 2.83
	0.5	$(10, 10, \sigma = 1.5)$	19.49 ± 1.08	26.06 ± 3.39	25.88 ± 3.16	$\mathbf{27.08 \pm 2.75}$	11.05 ± 0.20
		$(30, 30, \sigma = 4.5)$	24.55 ± 2.47	23.94 ± 3.61	23.77 ± 3.50	$\mathbf{24.67 \pm 3.30}$	11.81 ± 0.28
		$(60, 60, \sigma = 6.5)$	24.16 ± 3.16	23.21 ± 3.56	23.02 ± 3.50	23.47 ± 3.37	11.79 ± 0.35
0.05	0.05	$(10, 10, \sigma = 1.5)$	27.54 ± 1.47	30.40 ± 3.46	$\mathbf{30.76 \pm 3.47}$	30.55 ± 3.51	26.55 ± 1.20
		$(30, 30, \sigma = 4.5)$	26.67 ± 3.59	25.95 ± 3.67	26.10 ± 3.67	26.44 ± 3.64	25.86 ± 2.93
		$(60, 60, \sigma = 6.5)$	$\mathbf{25.03 \pm 3.74}$	24.48 ± 3.69	24.55 ± 3.68	24.91 ± 3.73	24.46 ± 3.22
	0.5	$(10, 10, \sigma = 1.5)$	27.54 ± 1.47	26.21 ± 3.51	26.02 ± 3.26	28.41 ± 3.62	12.00 ± 0.15
		$(30, 30, \sigma = 4.5)$	26.67 ± 3.59	24.01 ± 3.67	23.83 ± 3.54	25.01 ± 3.55	11.93 ± 0.27
		$(60, 60, \sigma = 6.5)$	25.03 ± 3.74	23.25 ± 3.59	23.07 ± 3.53	23.54 ± 3.40	11.84 ± 0.34

TABLE 2: PSNR values for various regularizers for different blur and noise parameters. The results are of form *mean*$\pm$*std*. The statistics are calculated for 150 random samples from the histology image

Noise	Lamda	Blur Kernel	L2	Laplacian	Maximize Cells	Cross Entropy	KL Divergence
0.15	0.05	$(10, 10, \sigma = 1.5)$	19.49 ± 1.08	20.90 ± 0.71	19.49 ± 1.08	19.48 ± 1.08	19.49 ± 1.08
		$(30, 30, \sigma = 4.5)$	24.55 ± 2.47	24.56 ± 2.47	24.55 ± 2.47	24.54 ± 2.46	24.55 ± 2.46
		$(60, 60, \sigma = 6.5)$	24.16 ± 3.16	24.16 ± 3.16	24.16 ± 3.16	24.15 ± 3.16	24.16 ± 3.16
	0.5	$(10, 10, \sigma = 1.5)$	19.51 ± 1.06	24.92 ± 1.04	19.49 ± 1.08	19.44 ± 1.08	19.46 ± 1.08
		$(30, 30, \sigma = 4.5)$	24.57 ± 2.47	24.62 ± 2.50	24.55 ± 2.47	24.46 ± 2.41	24.52 ± 2.45
		$(60, 60, \sigma = 6.5)$	$\mathbf{24.17 \pm 3.17}$	24.16 ± 3.17	24.16 ± 3.16	24.12 ± 3.16	24.13 ± 3.15
0.05	0.05	$(10, 10, \sigma = 1.5)$	27.54 ± 1.47	28.53 ± 1.53	27.54 ± 1.47	27.50 ± 1.46	27.53 ± 1.47
		$(30, 30, \sigma = 4.5)$	$\mathbf{26.68 \pm 3.59}$	26.67 ± 3.59	26.67 ± 3.59	26.67 ± 3.57	$\mathbf{26.68 \pm 3.59}$
		$(60, 60, \sigma = 6.5)$	$\mathbf{25.03 \pm 3.74}$	$\mathbf{25.03 \pm 3.74}$	$\mathbf{25.03 \pm 3.74}$	25.00 ± 3.71	$\mathbf{25.03 \pm 3.73}$
	0.5	$(10, 10, \sigma = 1.5)$	27.58 ± 1.47	$\mathbf{30.25 \pm 2.89}$	27.54 ± 1.47	27.20 ± 1.42	27.31 ± 1.43
		$(30, 30, \sigma = 4.5)$	$\mathbf{26.69 \pm 3.60}$	26.63 ± 3.61	26.67 ± 3.59	26.55 ± 3.46	26.63 ± 3.52
		$(60, 60, \sigma = 6.5)$	$\mathbf{25.04 \pm 3.74}$	25.02 ± 3.74	25.03 ± 3.74	24.68 ± 3.38	24.87 ± 3.57

TABLE 3: PSNR values for various regularizers for different blur and noise parameters. The results are of form *mean*$\pm$*std*. The statistics are calculated for 150 random samples from the histology image

Noise	Lamda	Blur Kernel	No Prior	Anisotropic TV	Isotropic TV	Hessian Schatten	L1
0.15	0.05	$(10, 10, \sigma = 1.5)$	0.25 ± 0.08	$\mathbf{0.61 \pm 0.04}$	0.59 ± 0.05	0.59 ± 0.06	0.24 ± 0.08
		$(30, 30, \sigma = 4.5)$	0.52 ± 0.08	$\mathbf{0.57 \pm 0.16}$	$\mathbf{0.57 \pm 0.15}$	0.54 ± 0.10	0.53 ± 0.08
		$(60, 60, \sigma = 6.5)$	$\mathbf{0.51 \pm 0.14}$	0.49 ± 0.18	0.50 ± 0.18	0.50 ± 0.15	$\mathbf{0.51 \pm 0.14}$
	0.5	$(10, 10, \sigma = 1.5)$	0.25 ± 0.08	0.58 ± 0.14	0.59 ± 0.15	$\mathbf{0.66 \pm 0.08}$	0.17 ± 0.07
		$(30, 30, \sigma = 4.5)$	0.52 ± 0.08	0.44 ± 0.17	0.45 ± 0.19	0.50 ± 0.14	0.42 ± 0.07
		$(60, 60, \sigma = 6.5)$	$\mathbf{0.51 \pm 0.14}$	0.39 ± 0.17	0.40 ± 0.19	0.41 ± 0.15	0.45 ± 0.13
0.05	0.05	$(10, 10, \sigma = 1.5)$	0.62 ± 0.08	0.80 ± 0.09	0.81 ± 0.09	$\mathbf{0.82 \pm 0.07}$	0.61 ± 0.08
		$(30, 30, \sigma = 4.5)$	0.64 ± 0.13	0.59 ± 0.17	0.59 ± 0.17	0.63 ± 0.14	0.64 ± 0.13
		$(60, 60, \sigma = 6.5)$	0.55 ± 0.17	0.50 ± 0.19	0.50 ± 0.19	0.54 ± 0.17	0.55 ± 0.17
	0.5	$(10, 10, \sigma = 1.5)$	0.62 ± 0.08	0.58 ± 0.15	0.59 ± 0.16	0.73 ± 0.11	0.47 ± 0.08
		$(30, 30, \sigma = 4.5)$	0.64 ± 0.13	0.44 ± 0.17	0.45 ± 0.19	0.52 ± 0.15	0.57 ± 0.13
		$(60, 60, \sigma = 6.5)$	$\mathbf{0.55 \pm 0.17}$	0.39 ± 0.17	0.40 ± 0.19	0.41 ± 0.15	0.51 ± 0.17

TABLE 4: SSIM values for various regularizers for different blur and noise parameters. The results are of form *mean*$\pm$*std*. The statistics are calculated for 150 random samples from the histology image

Noise	Lamda	Blur Kernel	L2	Laplacian	Maximize Cells	Cross Entropy	KL Divergence
0.15	0.05	$(10, 10, \sigma = 1.5)$	0.25 ± 0.08	0.30 ± 0.10	0.25 ± 0.08	0.25 ± 0.08	0.25 ± 0.08
		$(30, 30, \sigma = 4.5)$	0.52 ± 0.08	0.52 ± 0.08	0.52 ± 0.08	0.53 ± 0.08	0.52 ± 0.08
		$(60, 60, \sigma = 6.5)$	$\mathbf{0.51 \pm 0.14}$	$\mathbf{0.51 \pm 0.14}$	$\mathbf{0.51 \pm 0.14}$	$\mathbf{0.51 \pm 0.14}$	$\mathbf{0.51 \pm 0.14}$
	0.5	$(10, 10, \sigma = 1.5)$	0.25 ± 0.08	0.48 ± 0.10	0.25 ± 0.08	0.25 ± 0.08	0.25 ± 0.08
		$(30, 30, \sigma = 4.5)$	0.52 ± 0.08	$\mathbf{0.53 \pm 0.08}$	0.52 ± 0.08	$\mathbf{0.53 \pm 0.08}$	$\mathbf{0.53 \pm 0.08}$
		$(60, 60, \sigma = 6.5)$	$\mathbf{0.51 \pm 0.14}$	$\mathbf{0.51 \pm 0.14}$	$\mathbf{0.51 \pm 0.14}$	$\mathbf{0.51 \pm 0.14}$	$\mathbf{0.51 \pm 0.14}$
0.05	0.05	$(10, 10, \sigma = 1.5)$	0.62 ± 0.08	0.66 ± 0.08	0.62 ± 0.08	0.61 ± 0.08	0.62 ± 0.08
		$(30, 30, \sigma = 4.5)$	0.64 ± 0.13	0.64 ± 0.13	0.64 ± 0.13	$\mathbf{0.65 \pm 0.13}$	0.64 ± 0.13
		$(60, 60, \sigma = 6.5)$	0.55 ± 0.17	0.55 ± 0.17	0.55 ± 0.17	$\mathbf{0.56 \pm 0.17}$	$\mathbf{0.56 \pm 0.17}$
	0.5	$(10, 10, \sigma = 1.5)$	0.62 ± 0.08	$\mathbf{0.77 \pm 0.05}$	0.62 ± 0.08	0.60 ± 0.08	0.60 ± 0.09
		$(30, 30, \sigma = 4.5)$	0.64 ± 0.13	0.64 ± 0.13	0.64 ± 0.13	$\mathbf{0.65 \pm 0.13}$	$\mathbf{0.65 \pm 0.13}$
		$(60, 60, \sigma = 6.5)$	$\mathbf{0.55 \pm 0.17}$	$\mathbf{0.55 \pm 0.17}$	$\mathbf{0.55 \pm 0.17}$	0.54 ± 0.15	$\mathbf{0.55 \pm 0.16}$

TABLE 5: SSIM values for various regularizers for different blur and noise parameters. The results are of form *mean*$\pm$*std*. The statistics are calculated for 150 random samples from the histology image